Journal of the European Ceramic Society 21 (2001) 2267–2274

www.elsevier.com/locate/jeurceramsoc

RBAO membranes/catalyst supports with enhanced permeability

Cavus Falamaki *, Alireza Aghaei, Navid Razavi Ardestani

Materials and Energy Research Center, PO Box 14155-4777, Tehran, Iran

Received 9 August 2000; received in revised form 28 December 2000; accepted 12 January 2001

Abstract

Conducting the RBAO process through the liquid-gas reaction regime could be an appropriate route to produce alumina membranes/supports. Such ceramic structures have a larger permeability compared to conventional alumina membranes and, at the same time, do posses high flexural strength. The initial Al content in the Al/Al_2O_3 mixture powder to be milled strongly affects permeability (negative), flexural strength (positive) and, to a lesser extent, porosity (negative) of the fired samples. Oxidation during milling is low (<6 wt.%), but strongly depends on the initial Al content.

Keywords: Al_2O_3; Membranes; Microstructure-final; Permeability; Strength

1. Introduction

In recent years, there has been an increasing interest in the application of ceramic membranes, alumina microporous membranes being one of the most important candidates. Inorganic membranes exhibit unique physical and chemical properties like thermal and structural stability, high resistance to chemical and microbiological attack and good backflush characteristics.[1] However, improvements are still needed in the area of mechanical properties, simpler processing and better and finer pore size.[2]

Recently, Luyten et al.[3] synthesized alumina membrane supports by the RBAO process with higher strength compared to the more conventional Al_2O_3 ones with comparable porosity, but they did not report any permeability data. Two of the main items in their procedures were: (I) Al content of 40 wt.% in the initial powder mixture and (II) relatively long milling times (>5 h). Although different values for the Al content in the initial powder to be milled have been reported,[4–6] the effect of such variations in the RBAO route on physical characteristics of the sintered final porous support membrane, like flexural strength and permeability have not been previously individually considered. This will be considered in this paper along with the effect of the sintering temperature and compaction pressure. A relatively short milling time (1 h) was implemented intentionally to restrict the oxidation reaction of Al to the heat treatment in the liquid-gas regime. Such a treatment results in the formation of crater-like defects, due to a melt coagulation or sweating of Al above its melting point.[7] As will be discussed, we have made use of this phenomenon in order to increase the permeability of the membranes while keeping high flexural strength. As far as microfiltration characteristics are concerned, samples synthesized by our method may be appropriate candidates for liquid separations (like serum sterilization) due to enhanced permeability. Then, the limiting factors will be reasonable strength and proper mean pore diameter. On the other hand, bimodal pore size ceramic structures may be used as catalyst supports due to their high permeability, strength and internal area. Also, such microstructures may act as ghosts for the encapsulation of active molecules, of interest in inclusion chemistry.

2. Experimental procedure

The starting materials for the RBAO process were α-alumina powder (99.8 wt.% Al_2O_3, average grain size 1.6 μm, ZS-402/M, Martinswerk) and aluminum with an average grain size of 38 μm supplied by MERCK. The milling fluid was acetone (MERCK). Six mixtures with the Al wt.% 15, 20, 25, 30, 35 and 40 were prepared. Each mixture was wet milled for 1 h in a planetary mill

* Corresponding author. Fax: +98-21-877-3352.
E-mail address: cavus-flamki@yahoo.com (C. Falamaki).

0955-2219/01/$ - see front matter
PII: S0955-2219(01)00094-2

(Fritsch) using 80 cm^3 acetone, 160 g Al/Al_2O_3 powder and 14 alumina balls (2 cm diameter) in alumina jars with an approximately total charge of 300 cm^3. The slip concentration had been optimized to obtain the desired final product size distribution. The milled powders were dried in air (24 h, 60°C) and fast milled for 1 min to get rid of agglomerates due to the drying procedure. In each case, 1 g of this powder was uniaxially pressed (two forming pressures 95.5 and 191.0 MPa) to form disks with a diameter of 20 mm (five samples for each experiment). The pressures applied gave sound compacts without cracks or delamination on ejection. The green compacts were thermally treated in air according to the following heating cycle: heating with a rate of 10°C/min up to 1100°C, isothermal holding for 1 h (oxidation step), heating with a rate of 5°C/min up to the sintering temperature, and an isothermal heating at the sintering temperature (1250, 1300, 1350, 1400 and 1450°C) for 2.5 h.

Except for the milling and drying step, the same procedure was performed for the alumina powder to produce conventional alumina membranes (sintering temperature 1450°C).

Phase and microstructure analysis of the final samples was done by X-ray diffraction (Siemens D500 Diffractometer) and SEM (Stereo Scan 360-Leica, Cambridge). Density and porosity were measured according to ASTM C 373. Dry and wet (water) permeability measurements were performed according to ASTM F 316, with a special holder[8] with a compressed air sealing facility made in our laboratory (Fig. 1). For the wet permeability tests, the samples were saturated with water by heating them in boiling water for 5 h and further cooling down and resting at room temperature for 24 h. Three point flexural strength measurements were performed on 1.2×20.0×7.0 mm rectangular bars with a mechanical testing machine (Instron model 1196). Powder particle size distribution measurements were accomplished using light scattering techniques (Fritsch, Analysette 22). Simultaneous thermogravimetric-differential thermal analysis (STA) was carried out using a Polymer Laboratories apparatus using a heating rate of 3°C/min.

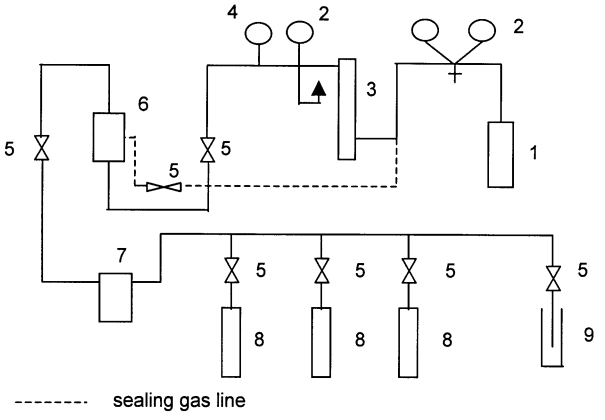

Fig. 1. Experimental configuration of the permeability measurements: (1) pressurized N_2 gas vessel, (2) pressure regulator, (3) silica gel moisture adsorber, (4) pressure gauge, (5) valve, (6) sample holder, (7) oil trap, (8) flowmeter, (9) bubble point test tube.

3. Results and discussion

3.1. Thermal analysis

The STA diagram of a milled powder (40 wt.% Al, forming pressure 95.5 MPa) is shown in Fig. 2. The initial weight loss under 300°C can be attributed to the loss of volatile matter, mainly H_2O and organic species.[7] The DTA curve shows that significant oxidation of Al begins near 400°C. The dominant reaction mechanism between 400 and 660°C is the solid–gas reaction of Al particles with the diffusing oxygen along grain boundaries through microcracks in the large particles and via macrocracks in the oxide skin of smaller particles.[6] At 660°C, unreacted Al melts and the oxidation reaction continues by a liquid–gas mechanism. The sharp exothermal peak around 825°C belongs to the liquid–gas oxidation reaction of aluminum. In producing dense RBAO ceramics, the process parameters are usually chosen so as to make the oxidation step take place in the solid-gas regime (up to 90% oxidation).[6] This is done by reducing the Al particle size under 1 μm during wet milling. Fig. 2 shows that the major part of the oxidation step occurs here in the liquid–gas regime. This is mainly due to the relatively short milling time used. The particle size distribution of a milled precursor is shown in Fig. 3. A bimodal distribution, with the larger particles attributed to Al is observed. The discrimination was done by the analysis of the backscatter SEM micrographs. The mean diameter of the Al particles is 1 μm and almost 40% are larger than 1 μm. Milled powders with different initial Al contents showed a very similar particle size distribution. According to Holz et al,[7] for the oxidation reaction to occur within the solid–gas domain, all the Al particles should be smaller than 1 μm. Therefore, referring to Fig. 3, the dominant liquid-gas reaction regime supported by STA is quite reasonable. On the other hand, due to the short milling time used, the milled powder mixture is assumed to be non-homogeneous. Then, during the compaction step, Al particles may contact each other and adhere to form particles larger than 1 μm. As it will be seen later, this fact is not only a drawback, but also an advantage as it leads to increased permeabilities. Near 900°C, weight changes stop, showing the end of the oxidation process, which is also supported by the DTA curve. Actually, the amount of Al oxidized to γ-alumina up to this point is less than 90%. A representative sample of each group of the sintered compacts was further heated at 1450°C for 2 h. Except for the samples initially sintered at 1250°C, no weight increase

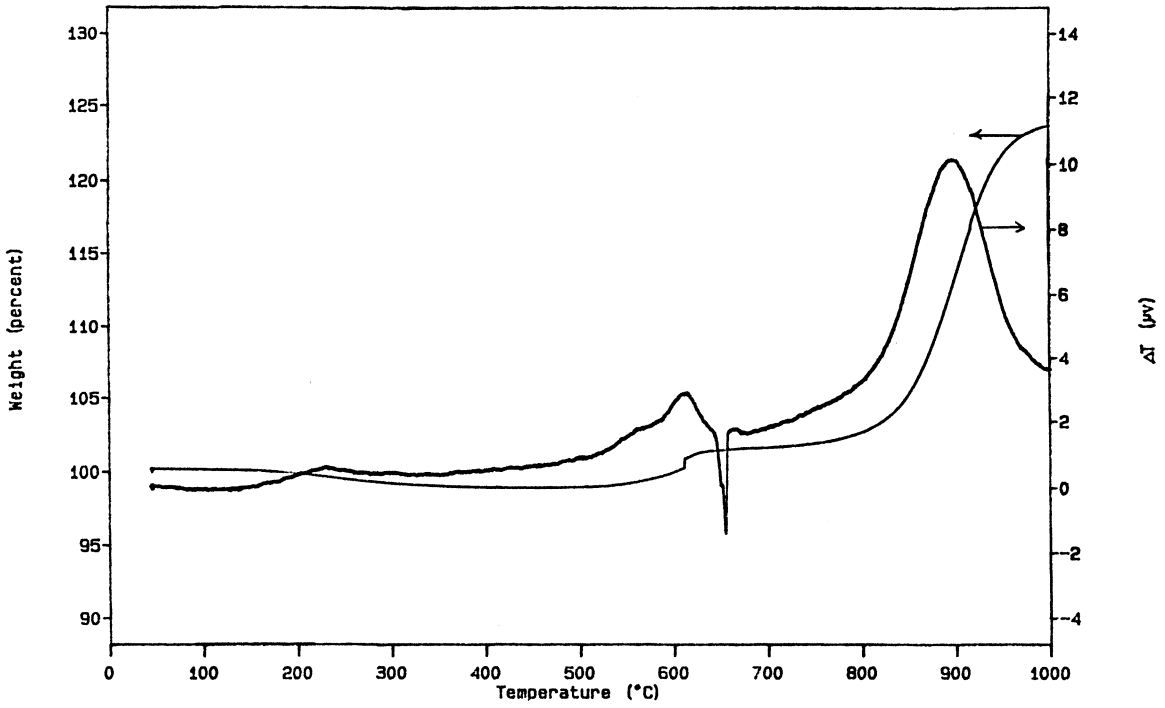

Fig. 2. STA analysis of a milled powder (35 wt.% Al content, compaction pressure 95.5 MPa).

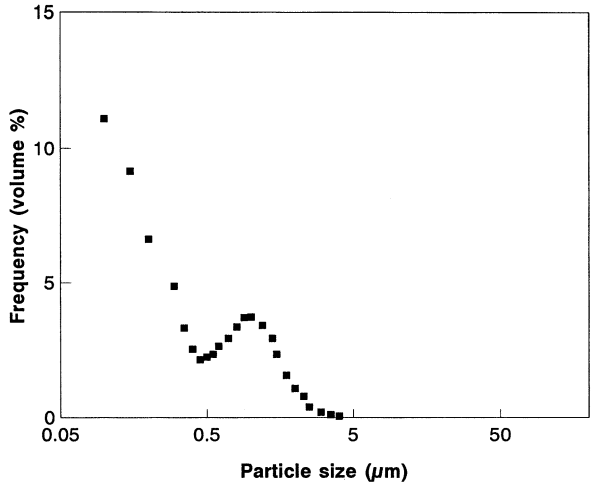

Fig. 3. Particle size distribution for a powder (35 wt.% Al) milled for 1 h.

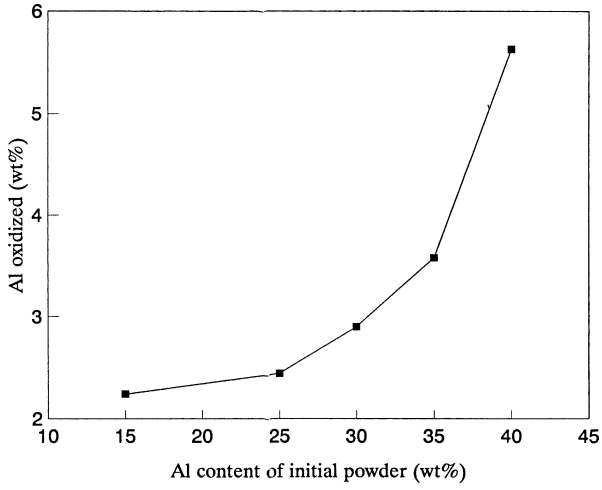

Fig. 4. Relationship between amount Al oxidized in mill and Al content in the initial powder.

was observed. This showed that the samples sintered at 1250°C still contained elemental Al.

During the milling procedure, some of the Al undergoes a hydrolysis reaction due to the water picked up by the acetone during the process. The amount of Al oxidation during the wet-milling step could be calculated considering the difference between the theoretical and observed weight gain after each heating cycle. This calculation was performed for the samples sintered at 1300, 1350, 1400 and 1450°C, for which the oxidation reaction was complete. TG analysis of milled powders with different Al contents showed an initial weight loss less than 1%, which we neglected in our computations. A curious observation is the trend of the Al content oxidized versus initial Al content in the initial charge (Fig. 4) during milling, which shows a strong increase in the oxidation with the increase in the Al content of the initial powder. This can be explained by the fact that increasing the Al content (total charge volume almost constant, 300 cm^3), increases the Al exposed surface per unit volume of the reaction system and thus accelerates the oxidation reaction.

3.2. Membrane/support synthesis

3.2.1. Influence of process parameters

The effect of the precursor Al content on the permeability of the sintered products for two initial forming pressures for different sintering temperatures are shown in Figs. 5 and 6. The permeability of conventional alumina membranes (zero Al content) is also included for comparison. In all cases the increase in the Al content results in a decrease in the permeability. Between 15 and 30 wt.% Al content, the dependence is sharp and after 30 wt.% it seems to slow down. The permeability of the 191.0 MPa pressed compacts is always lower than that of the 95.5 MPa ones. The largest difference between the two pressures occurs at the least Al content (15 wt.%) and may reach values near 40×10^{-11} m^5/N min (at 1450 and 1400°C sintering temperatures).

Wet permeability tests were based on the fact that a wet membrane will pass air when the applied air pressure exceeds the capillary attraction of the fluid in the pores. A simple formula relates this pressure to the capillary pore diameter:

$$P = 4\gamma\cos\alpha/d \quad (1)$$

where γ is surface tension of the wetting fluid, α angle of contact, P air pressure and d the capillary diameter.

A typical flow rate versus pressure diagram for the dry and wet membrane experiments is shown in Fig. 7. The shape of the wet flow curve is approximately a straight line, and this happens when all the permeable pores are equivalent in size.[10] The effective pore diameter in this case, will be the size pertaining to the pressure at which the first continuous flow through the membrane is detectable (point B on Fig. 7). The permeability is controlled by bottlenecks and this is made clear in the following paragraph.

Consider the two porous structures shown in Fig. 8. Structure (a) consists of a microporous matrix with a mean pore size d_1 and structure (b) is the same as (a) but having an even distribution of macropores with the size of d_2 within the matrix. Wet permeability tests will result in straight lines for both (a) and (b) structures and the effective pore diameter will be the same, i.e. d_1. This is because for pores of different sizes and in series, the smallest permeable pores will be the controlling ones. Thus, if the structure consists of macropores embedded in a microporous matrix consisting of equivalent size pores, by wet permeability tests only the mean permeable pore size of the matrix could be evaluated.

Considering Figs. 9 and 10, the existence of relatively large hollow channels (10–200 μm) in our RBAO products is clear. Their concentration increases with the increase of the Al content in the initial powder. Such channels have also been reported before and are probably

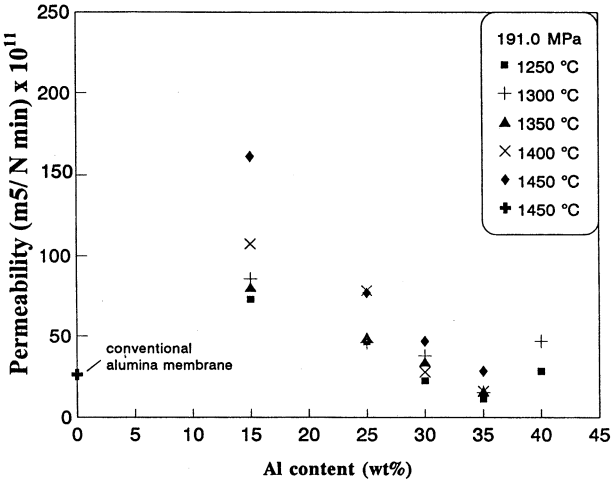

Fig. 6. Permeability of sintered products as a function of Al content for a compaction pressure of 191.0 MPa.

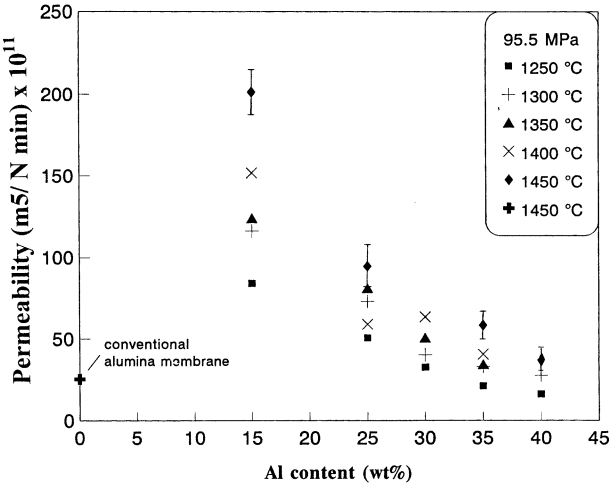

Fig. 5. Permeability of sintered products as a function of Al content for a compaction pressure of 95.5 MPa.

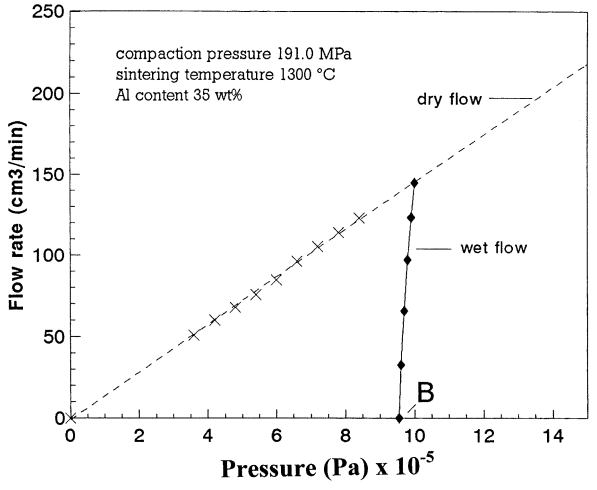

Fig. 7. Typical flow rate versus pressure for the dry and wet flow experiments.

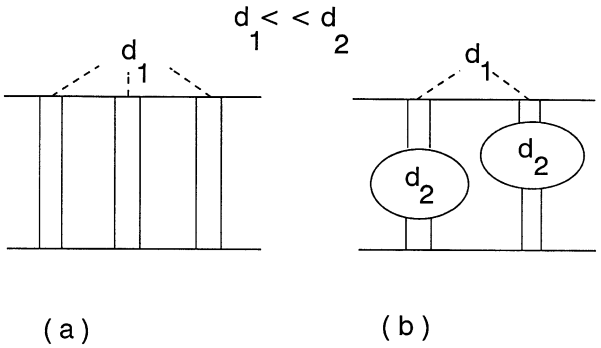

Fig. 8. A simple representation of two permeable structures having the same controlling permeable pore size.

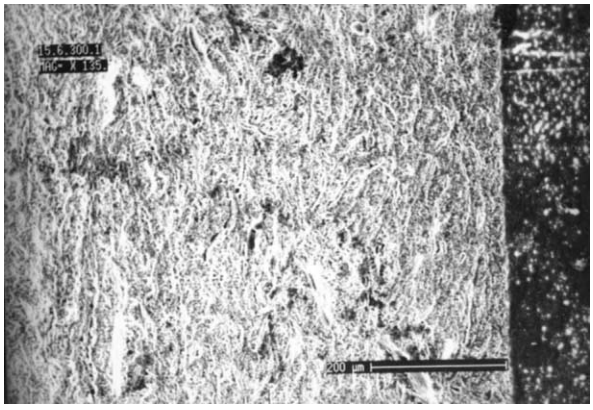

Fig. 9. Microstructure of an RBAO porous body with initial Al content of 15 wt.%, sintering temperature 1300°C and compaction pressure of 191.0 MPa.

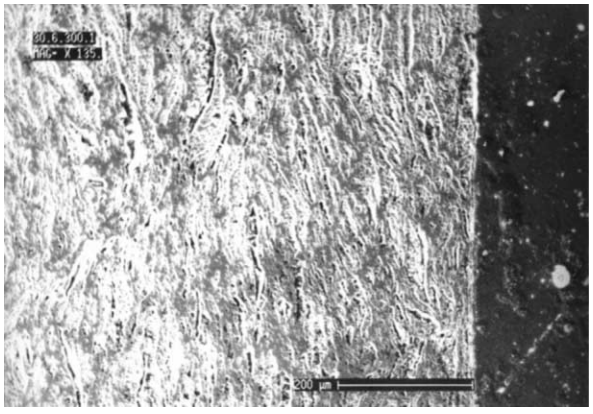

Fig. 10. Microstructure of an RBAO porous body with initial Al content of 30 wt.%, sintering temperature 1300°C and compaction pressure of 191.0 MPa.

due to melt coagulation or sweating of the Al above its melting point during the RBAO process.[4] These pores resemble cracks in ceramic systems (like Si_3N_4) due to fracture under tensile and compressive cyclic loads. In these systems, crack growth is promoted by the viscous flow of amorphous films along grain boundaries and interfaces.[11] In our RBAO system, crack growth is promoted by the pushing viscous flow of the aluminum melt (11.5% volume expansion during phase change) along the micropore system. Macropore production is also enhanced by the relatively high heating rate applied (10°C/min). We suppose that the low milling time resulting in incomplete homogenization of the milled powder and the existence of Al particles larger than 1 mm are the main reasons for melt coagulation. In contrast to Lutyen et al.,[4] we do not consider these large channels as structural defects as, referring to Figs. 14 and 15 (to be considered later), the flexural strength of the final products is quite high enough. The existence of these large channels improves the total permeability for most of the specimens. Our tests showed that in all cases, the wet permeability curves could be approximated with straight lines and corresponding to diameters less than 1 mm. Thus, although these large cavities are present, the controlling pore diameter, characteristic for separation purposes, is the effective pore diameter, which is always lower than 1 mm [structure (b)]. This is due to the encapsulation of the macrocraks within the RBAO body, which is approximately well ordered. This order is due to the plate-like arrangement of Al particles vertical to the press axis during the compaction step. Thus, for size exclusion purposes, macrocracks lower the total diffusion resistance and the RBAO matrix acts as a sieve (macrocracks excluded).

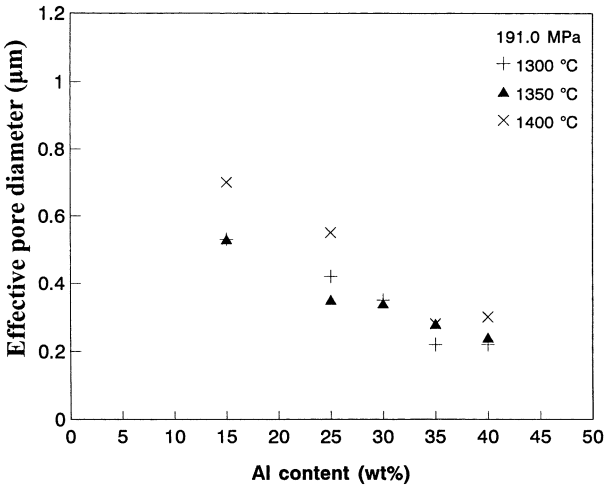

Fig. 11. Effective pore diameter as a function of Al content in the initial powder for a compaction pressure of 191.0 MPa.

With the increase of the Al content, the plasticity and pressability of the milled powder increases and results in smaller porosity of the green compacts. Also, lamination in the direction vertical to the press axis (which could be easily observed during the experiments) results in a drastic decrease in the number and size of channel pores. Fig. 11 shows that the effective pore diameter decreases significantly with Al content increase. It is quite clear that increase in the green compact porosity has a direct effect on the sintered products, and hence on their permeabilities.

Figs. 12 and 13 show the porosity versus Al content for the sintered products for 5 different sintering temperatures and two forming pressures. A slight decrease of the porosity with Al content increase is observed. On the other hand, measurement of the volume change of the samples was observed to be positive and to reach values up to 25%. As the Al content increase is accompanied with more macrocrack formation, we should have porosity increase due to the void volume increase. On the contrary, the porosity decreases. This can be explained by considering the fact that oxidation of the Al in the matrix is accompanied by a volume increase (28% for Al to α-Al_2O_3 transformation) which results in the filling of the existing pores. This compensates the positive effect of macrocrack formation on the porosity.

For each initial forming pressure, and constant Al wt.%, increasing the sintering temperature leads to an increase in the permeability. This is more pronounced for lower levels of Al concentrations. At this stage, it should be noted that after the oxidation step at 1100°C, the system consists of a binary mixture of alumina particles: Coarse ones originating from the initial Al/Al_2O_3 powder (primary particles), and very fine and active ones, nucleated and grown during the oxidation of Al to γ-Al_2O_3 and its transformation into α-Al_2O_3 (secondary particles). During the sintering stage, the secondary alumina particles, due to their high activity, readily undergo sintering, adhering to the relatively large primary alumina particles by extinguishing small channels and thus increasing the larger pore diameter. Thus, by increasing the sintering temperature we have an increase in permeability. This trend is followed for both of the compaction pressures applied. As a clear postulate, high forming pressures are preferably avoided as they make oxidation difficult and lower the permeability, especially in ineffectively milled powders. Thus, by increasing the

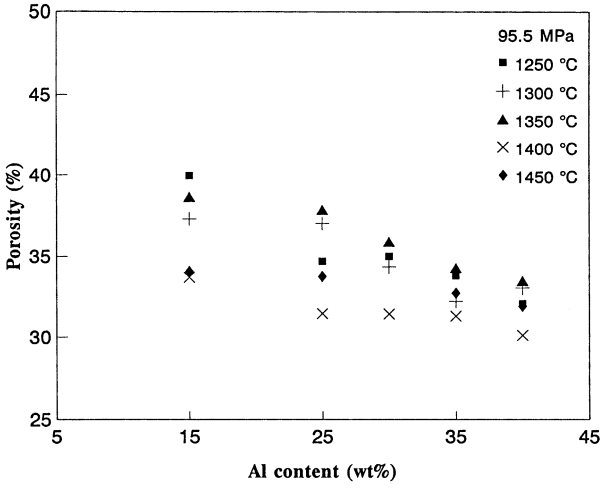

Fig. 12. Relationship between porosity and Al content in the initial powder for a compaction pressure of 95.5 MPa.

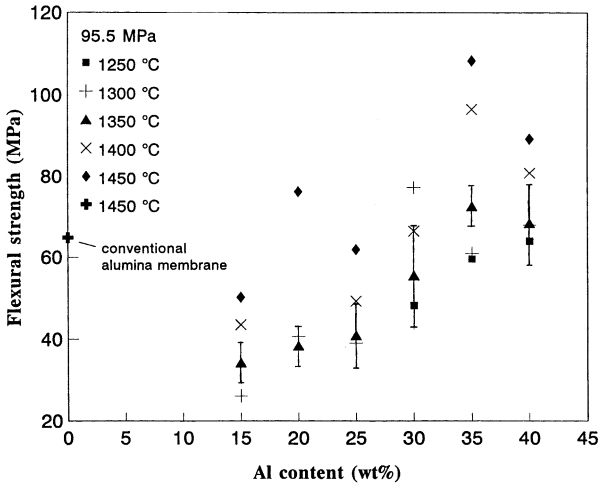

Fig. 14. Flexural strength as a function of Al content at different temperatures for a compaction pressure of 95.5 MPa.

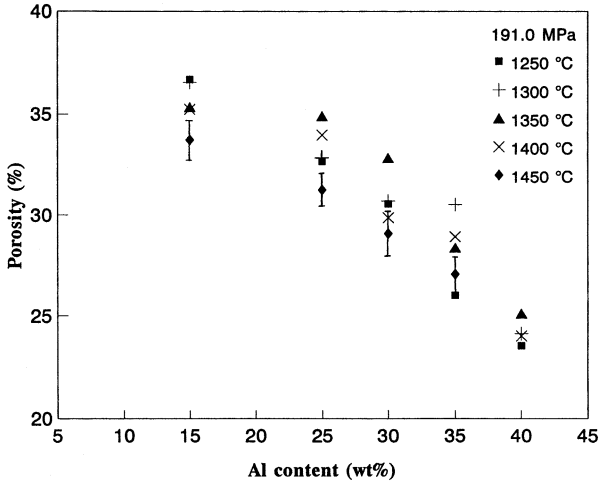

Fig. 13. Relationship between porosity and Al content in the initial powder for a compaction pressure of 191.0 MPa.

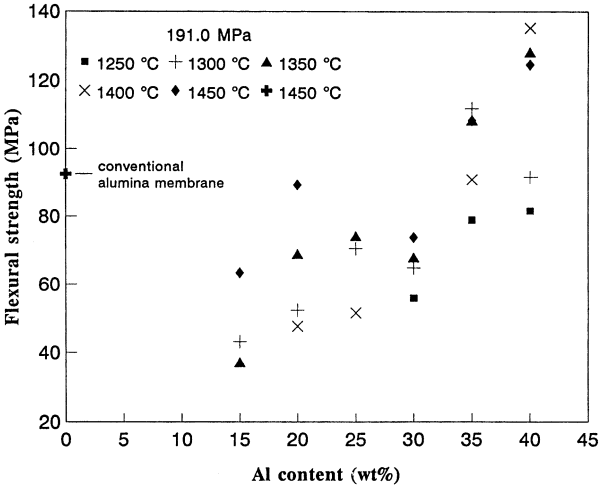

Fig. 15. Flexural strength as a function of Al content at different temperatures for a compaction pressure of 191.0 MPa.

sintering temperature we have an increase in permeability due to a higher effective pore diameter.

3.2.2. Flexural strength

Figs. 14 and 15 show the flexural strength of the sintered products versus Al content in the initial powder. The major result is that increasing the Al content has a positive effect on strength along with the fact that higher sintering temperatures result in higher strengths. Figs. 16 and 17 show the improved bonding of alumina particles due to higher temperatures. This can be attributed to 1) the existence of more bonds in the initial green compact due to a higher content of the ductile Al particles (Al/Al contacts)[9] and (2) the enhanced sintering due to the formation of the very active secondary particles during the oxidation and early during the sintering stage. This is also consistent with the effective pore diameter measurements, which show that increasing Al content results in a matrix with significantly smaller pores. As a matter of fact, the flexural strength of an alumina disk produced with the same procedure and having quite the same porosity is lower than that of the RBAO synthesized material (Table 1), which confirms the results of Luyten et al.[3] It should be noted that due to the use of little bars for the three-point test, the strength values obtained are somewhat lower than the real ones, although consistent with each other.

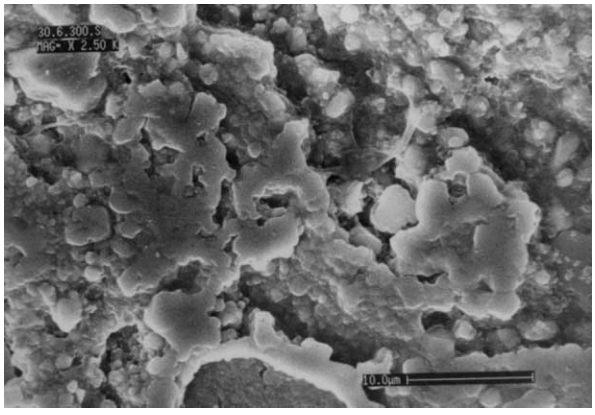

Fig. 16. Microstructure of an RBAO porous body with initial Al content of 30 wt.%, sintering temperature 1300°C and compaction pressure of 191.0 MPa.

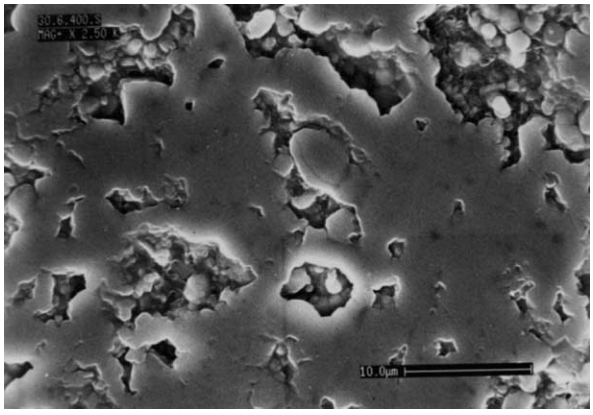

Fig. 17. Microstructure of an RBAO porous body with initial Al content of 30 wt.%, sintering temperature 1400°C and compaction pressure of 191.0 MPa.

Table 1
Comparison between flexural strength of simple and RBAO products

Product[a]	Porosity (vol.%)	Permeability (m^5/N min)	Three-point flexural strength (MPa)
Conventional alumina	35.73	25.42	64.77
RBAO	32.73	58.296	108.5

[a] Sintered at 1450°C, 95.5 MPa compaction pressure.

4. Conclusions

It has been shown that conducting the RBAO process through the liquid–gas reaction regime could be an appropriate route to produce alumina membranes/supports. Such ceramic structures have a larger permeability compared to conventional alumina membranes and, at the same time, do posses high flexural strength. The initial Al content in the Al/Al_2O_3 mixture powder to be milled strongly affects permeability (negative), flexural strength (positive) and, to a lesser extent, porosity (negative) of the fired samples. Oxidation during milling is low (<6 wt.%), but strongly depends on the initial Al content. In all experiments, increasing the compaction pressure had a negative effect on the final structure. High sintering temperatures result in higher strength and permeabilities. Obviously, to design a membrane/support with the desired properties, an optimization of the process parameters, Al content, compaction pressure and sintering temperature is needed.

References

1. Hsieh, H. P., Bhave, R.R. and Fleming, H.L., Microporous alumina membranes. *J. Mem. Sci.*, 1988, **39**, 221–241.
2. Chan, K. and Brownstein, A., Ceramic membranes — growth prospects and opportunities. *Am. Ceram. Soc. Bull., American Ceramic Society*, 1991, **70**(4), 703–707.
3. Luyten, J., Cooymans, J. and Leysen, R., Shaping of a RBAO-membrane support. In *Key Engineering Materials*, Vols. 132–136, ed. V. Ecers. Trans. Tech. Publications, Switzerland, 1997, pp. 1691–1694.
4. Luyten, J., Cooymans, J., Diels, P. and Sleurs, J., RBAO-used as part of a membrane configuration. In: *Third Euro-Ceramics*, Vol. 1, ed. P. Duran and J. F. Fernandez. Faenza Editrice Iberica, S.L., Spain, 1993, p. 657.
5. Luyten, J., Cooymans, J., Smolders, C., Vercauteren, S., Vansant, E. F. and Leysen, R., Shaping of multilayer ceramic membranes by dip coating. *J. Eur. Ceram. Soc.*, 1997, **17**, 273–279.
6. Wu, S., Holz, D. and Claussen, N., Mechanisms and kinetics of

reaction-bonded aluminum oxide ceramics. *J. Am. Ceram. Soc.*, 1993, **76**(4), 970–980.
7. Holz, D., Wu, S., Scheppokat, S. and Claussen, N., Effect of processing parameters on phase and microstructure evolution in RBAO ceramics. *J. Am. Ceram. Soc.*, 1994, **77**(10), 2509–2517.
8. Falamaki, C., Aghaei, A. and Ardestani, N. R., Iranian Patent 26 446, 2000.
9. Claussen, N., Wu, S. and Holz, D., Reaction bonding of aluminum oxide (RBAO) composites: processing, reaction mechanisms and properties. *J. Eur. Ceram. Soc.*, 1994, **14**, 97–109.
10. Roy, S. K., Characterization of porosity in porcelain-bonded porous alumina ceramics. *J. Am. Ceram. Soc.*, 1969, **52**(10), 543–547.
11. Ramamurty, U., Hansson, T. and Suresh, S., High-temperature crack growth in monolithic and SiC reinforced silicon nitride under static and cyclic loads. *J. Am. Ceram. Soc.*, 1994, **77**(11), 2985–2999.